Electronic Supplementary Material (ESI) for Physical Chemistry Chemical Physics.

Supporting Information

New Insights into a Hydrogen Bond: Hyper-Raman Spectroscopy of DMSO-Water Solution

Christopher B. Marble,*[,a] Xingqi Xu,[b,c] Georgi I. Petrov,[b] Dawei Wang,[c] Vladislav V. Yakovlev[a,b]

[a] Department of Physics and Astronomy, Texas A&M University, College Station, Texas, 77843, USA.
[b] Department of Biomedical Engineering, Texas A&M University, College Station, Texas, 77843, USA.
[c] Interdisciplinary Center for Quantum Information, State Key Laboratory of Modern Optical Instrumentation, and Zhejiang Province Key Laboratory of Quantum Technology and Device, Department of Physics, Zhejiang University, Hangzhou 310027, Zhejiang Province, China.
* Corresponding author
Email: cmarble112@tamu.edu

Table of Contents

1. Materials

1.1 Reagents

Samples of DMSO (Alfa Aesar #32434), DMSO-d_6 (Alfa Aesar #36517), D_2O (Aldrich #151882) and deionized H_2O (18.2 MΩ-cm resistance) were used as acquired.

1.2 Instruments

A custom-made high-power (> 6 W), high-repetition rate (3 MHz), mode-locked picosecond pulse (8 ps) laser (see Ref. 1 and Ref. 2 for specifications), The 1064 nm light was frequency doubled using a Lithium Tri-borate crystal. The laser light was focused into, and collected from, UV-grade quartz cuvettes using microscope objectives (Optosigma, 20 ×, 0.45 NA, EFL 8.0 mm and Thorlabs, 20 ×, 0.4 NA respectively). The UV light was then imaged onto the front slit of the spectrometer using a 10 cm achromatic UV lens. A HORIBA iHR 320 spectrometer with a 50 µm entrance slit and a Symphony II, 2048 × 512 px UV-enhanced liquid-nitrogen cooled charge-couple-device detector were used to collect the spectra in this experiment. Spectrometer calibration was performed with a StellarNet® SL2 Hg(Ar) calibration lamp.

2. Methods

2.1 Spectrometer Calibration and Resolution

A HORIBA spectrometer with a 50 µm entrance slit and a CCD detector was used to collect the spectra in this experiment. A calibration spectra was collected using a Hg(Ar) lamp using mercury and argon emission lines from 265 nm to 295 nm. A quadratic calibration curve was calculated using the observed peak locations and used to correct all measured spectra. The detector resolution was determined by measuring the fine structure of mercury at 265 nm and found to be consistent with simulated peaks with full width at half maximum (FWHM) of 0.05 nm. This corresponds to individual pixels have a resolution of ~2 cm^{-1}. By fitting the spectra, shifts in the center wavenumbers could be determined to within ~1 cm^{-1}.

2.2 Collection of Hyper-Raman Scattered Light

Fig. S1 illustrates a hyper-Raman spectroscopic setup, where a custom-made 1064 nm, 8 ps laser was used as excitation source. The samples, contained in quartz cuvettes, were illuminated by focused 532 nm laser pulses generated by frequency-doubling the 1064 nm light from the Nd: YVO_4 seed laser in a Lithium Tri-borate crystal. The excitation light was focused into the cuvette using a microscopic objective. As depicted in Fig. S1, scattered light was collected with an achromatic UV objective and imaged onto the front slit of the spectrometer using a 10 cm achromatic UV lens.

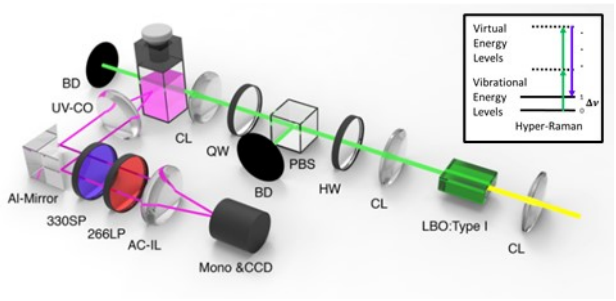

Fig. S1. The experimental setup for hyper-Raman scattering. The insert shows a vibrational mode of the sample (Δν) being probed via IR absorption, Raman and hyper-Raman scattering. Abbreviations: collimating lens (CL), half wave plate (HW), polarizing beam splitter (PBS), focusing lens (FL), achromatic UV collection objective (UV-CO), Beam dump (BD), short pass edge filter at 330 nm (330SP), long pass edge filter at 266 nm (266LP), aluminum mirror (Al-mirror), achromatic imaging lens (AC-IL), monochromator (mono).

2.3 Sample Preparation and Data Collection Procedure

DMSO-H_2O solutions were prepared by weight using an analytical balance.

To compare the peak amplitudes between measurements in a right-angle scattering experiment the alignment had to be optimized for each mixture. Liquid was added and removed via pipet without moving the quartz cuvette; however, the difference in optical properties in the liquids caused a slight shift in alignment that prevented accurate peak amplitude measurements. Hence the first step in the collection procedure for each sample was to verify the alignment was optimized by maximizing the hyper-Rayleigh signal. The hyper-Rayleigh line was recorded incase realignment shifted the spectra slightly on the CCD. The spectrometer grating was not moved between hyper-Rayleigh and hyper-Raman collections, instead a 266 nm long pass filter was used to suppress the hyper-Rayleigh line when hyper-

Raman scattering (HRS) spectra were recorded. By this procedure, DMSO-H_2O spectra were taken at an average power of 1.7 W for mixtures of 5.0 mol % increments with additional measurements of 1.0 mol % DMSO and 33.3 mol % DMSO (the eutectic point).
When performing measurements of intermediate concentrations at an average power of 1.7 W, self-focusing effects became visually evident as momentary flickers of Rayleigh scattered light. Measurement of the intensity of the hyper-Rayleigh line as a function of concentration at a power of 1.7 W (Fig. S2 left) showed a clear positive deviation with concentration from a simple linear combination of pure DMSO and H_2O responses (Signal = X*$Signal_{DMSO}$ + (1-X)*$Signal_{H2O}$). Reducing power to 1.0 W suppressed the self-focusing at the cost of significantly increasing the required collection times and resulted in a hyper-Rayleigh plot more consistent with the linear combination of pure responses anticipated (Fig. S2 right). Due to the sensitivity of the peak area measurements to laser power, the peak areas from the reduced power measurements are used in this article and supplement. Reduced power measurements were taken in increments of 10 mol % DMSO. The deviation of the hyper-Rayleigh line from the linear combination of pure DMSO and H_2O responses is assumed to be caused by sub-optimal alignment. For this reason, we used the deviation of the hyper-Rayleigh lines from the anticipated linear combination of responses as a correction factor when plotting and analyzing the hyper-Raman peak areas. Note the data in Fig. S2 is plotted after a Beer–Lambert law correction for the weak DMSO UV absorption at 266 nm for an estimated pathlength of 2 mm and that Beer–Lambert law corrections were performed for all hyper-Raman peak areas and hyperpolarizabilities reported. The absorption coefficients for all wavelengths were measured experimentally using a Thermo Scientific Genesys 10S UV-Vis spectrophotometer.

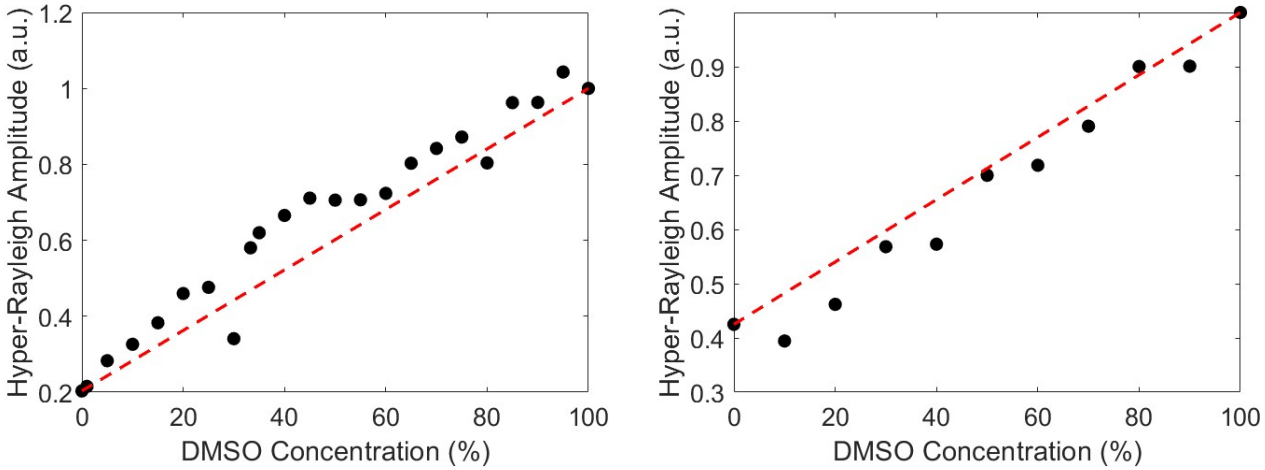

Fig. S2. Plot of the peak area of the hyper-Rayleigh signal as a function of concentration for average laser powers of 1.7 W (left) and 1.0 W (right). The red dashed lines represent a linear combination of pure DMSO and H_2O responses.

2.4 Background Subtraction and Peak Fitting

The collected HRS spectra were converted to wavenumbers using the measured hyper-Rayleigh lines. Fig. S3 top overlays the hyper-Rayleigh line and low wavenumber water translational modes against the HRS spectra collected with the long pass filter. A quadratic spectrometer response function was used to remove the background of the HRS spectra with background fit points chosen to not be affected by spectral features of either liquid. This quadratic background subtraction was necessary to make accurate calculations of peak areas and wavenumbers in low DMSO concentration solutions and pure H_2O. The Savitzky-Golay smoothed values at 1180 cm^{-1}, 1800 cm^{-1}, 2600 cm^{-1}, and 3800 cm^{-1} were used to calculate the fit for the DMSO-H_2O solution (see Fig. S3 bottom).

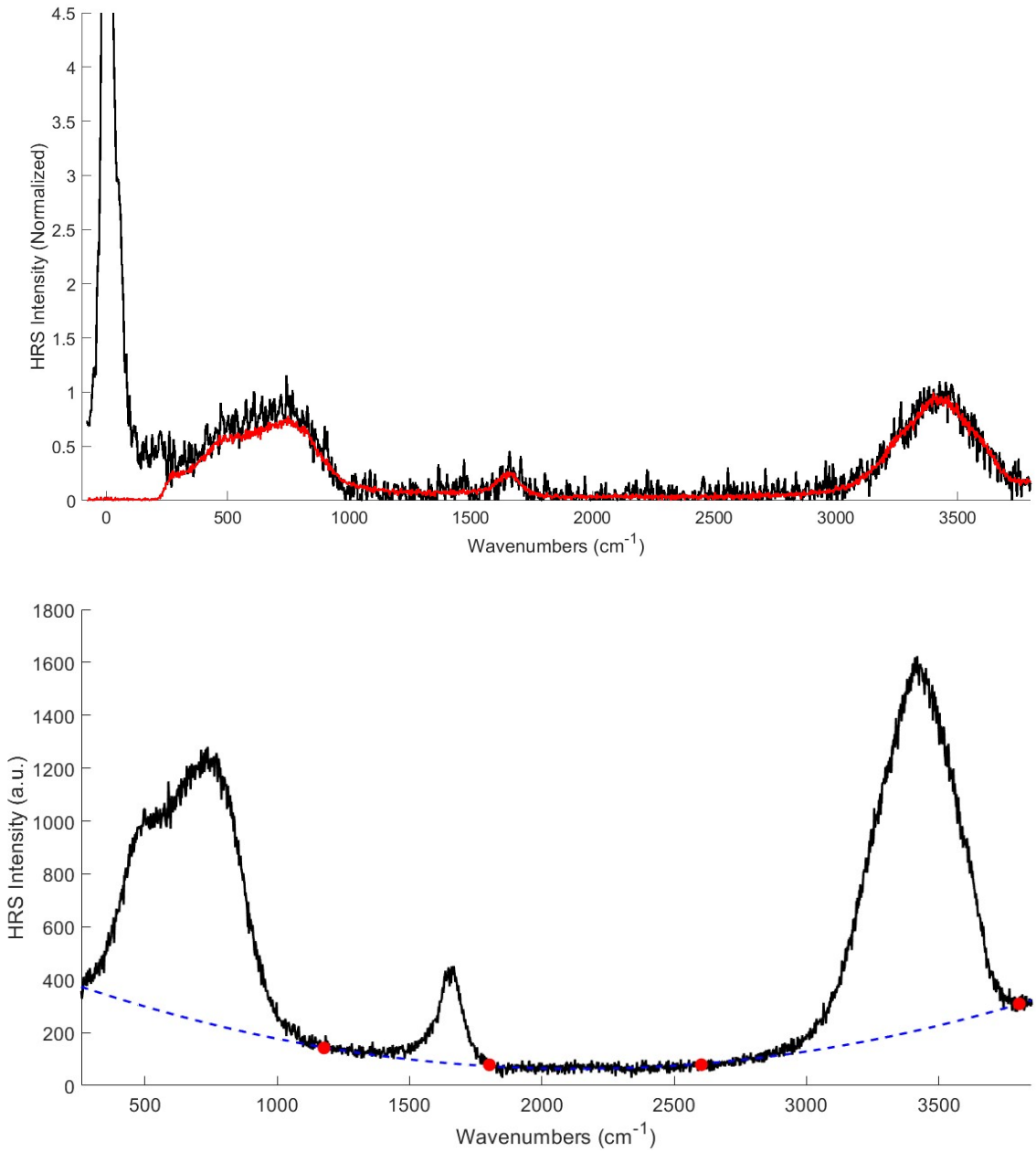

Fig. S3. Top: HRS spectra of water taken with the long pass filter (red) and without the filter (black). Bottom: Background subtraction for the HRS spectra of pure H_2O (black) using a quadratic fit (dashed blue line) calculated from four fitting regions (red circles). Note the 266 nm long pass filter was responsible for the decrease in signal below 300 cm^{-1} resulting in the signal falling below the background fit in this region.

The post-background subtraction spectra were fit with Gaussian peaks in MATLAB using the lsqcurvefit program. The initial Gaussian amplitudes, peak frequencies and FWHM for the fit were estimated by the user. In general, for DMSO the estimated amplitudes and frequencies were determined by identifying the peaks in the spectra with an estimated FWHM of ~20 cm^{-1}. For H_2O, the estimated values were taken from the tables and figures in Ref. 3. To determine the sensitivity of the fit to the initial conditions, 50 fits were performed with random variations to the initial parameters (generally +/- 20% changes in amplitude or FWHM and 5 cm^{-1} shifts in DMSO frequencies and 20 cm^{-1} – 50 cm^{-1} shifts in H_2O frequencies). The mean value and uncertainties of the reported amplitudes and wavenumbers are calculated from the result of the 50 fits. The 1000 cm^{-1} to 1100 cm^{-1} region was not fit as the numerous, overlapping peaks lie in that range so no conclusive peak assignments could be made for that region.

3. Supplemental Data and Figures

3.1 Hyper-Raman of Pure Spectra

In Fig. S4, the HRS spectra of DMSO, DMSO-d_6, H_2O and D_2O are plotted here with their responses annotated. In Table S1, the HRS spectral features of pure DMSO are identified, catalogued and compared to prior Raman and IR observations.[4–7] Notably, the intensity of the DMSO modes were different than IR and Raman spectra with inversions of the relative amplitudes of the symmetric and antisymmetric stretching modes of C-S (667 and 697 cm^{-1}) and C-H (2912 and 2997 cm^{-1}) compared to Raman spectra.[8]

The HRS spectra of H_2O and D_2O (Fig. 7) compare favorably with the HRS spectra reported in literature[3] with two strong, broad librational modes (511 and 758 cm^{-1} H_2O/373 and 568 cm^{-1} D_2O), and detectable bend (1655 cm^{-1} H_2O/1216 cm^{-1} D_2O), and stretch modes (3100-3600 H_2O/2300-2700 cm^{-1} D_2O).

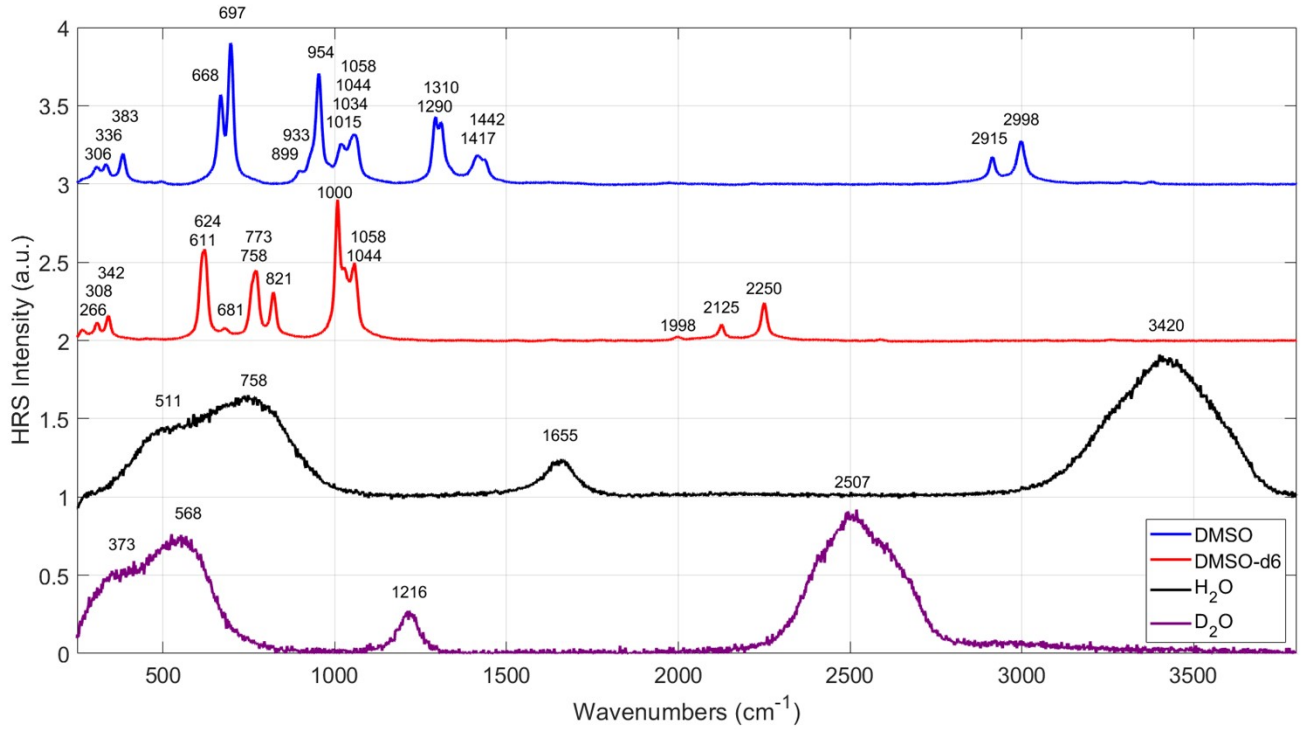

Fig. S4. The hyper-Raman spectra of DMSO (top), DMSO-d_6 (top-middle), H_2O (bottom-middle), and D_2O (bottom).

Table S1. Comparison of vibrational modes for liquid DMSO using hyper-Raman, Raman and infrared absorption.

Assignment	HRS (cm^{-1})	Raman (cm^{-1}) (Ref. 4)	IR (cm^{-1}) (Refs. 5–7)
C-S-C bending	306	309	309
C-S=O rocking (out-of-plane)	336	333	331
C-S=O rocking (in-plane)	383	382	381
C-S stretching (sym.)	668	667	667
C-S stretching (asym.)	697	698	697
Not assigned	899	-	890
Not assigned	933	-	930
C-H rocking	954	953	953
C-H rocking	1015,* 1034*	1019	1015, 1034
S=O stretching (multiple)	1044,* 1058*	1026, 1042, 1058	1042, 1058
H-C-H bending	1290	1307	-
H-C-H bending	1310	-	1310
H-C-H bending	1417	1417	1407
H-C-H bending	1442	-	1438
C-H stretching (sym.)	-	2809	-
C-H stretching (sym.)	2915	-	2912
C-H stretching (asym.)	2998	2994	2996

*The C-H and S=O modes between 1000 cm^{-1} and 1060 cm^{-1} cannot be resolved by HRS.

Abbreviations: sym=symmetric; asym=asymmetric

3.2 Hyper-Raman of DMSO-H_2O solutions

In Fig. S5, the HRS spectra of pure DMSO, pure H_2O and solutions of 75 mol %, 50 mol %, 33.3 mol % and 10 mol % DMSO are plotted.

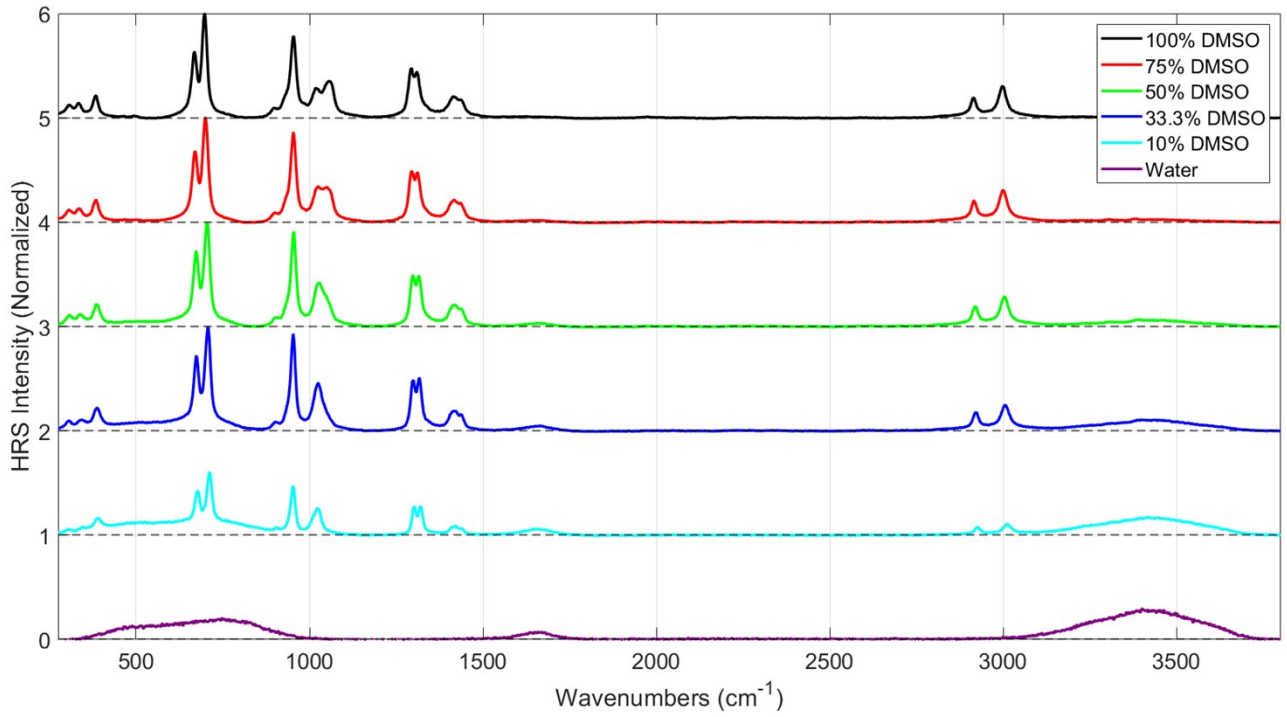

Fig. S5. The hyper-Raman spectra of DMSO-H_2O solutions as a function of DMSO concentration.

3.3 Overview of the Effect of H_2O on the DMSO Molecule

The addition of H_2O affects the electron charge distribution in the DMSO molecules. Below we show the red/blueshift of the bond frequencies as a function of DMSO concentration as a color graph (Fig. S6). This provides an overview and allows for rough comparison of the red/blueshift of the bond compared to other bonds. A table of wavenumber shifts and uncertainties is provided for concentrations of 75%, 50%, 33.3% and 10% DMSO (Table S2). In the following pages, we plot peak center wavenumbers and peak areas with uncertainties calculated from the fit algorithm.

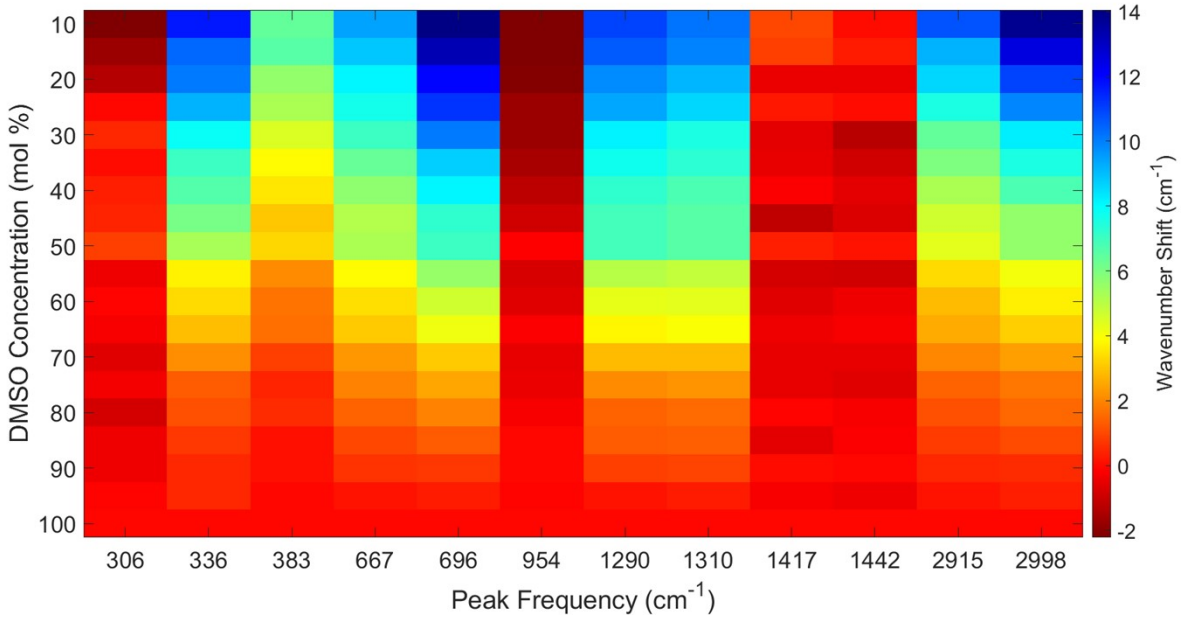

Fig. S6. A color plot of the red/blueshifts of different DMSO vibrational modes in response to dilution with H_2O.

Table S2. Observed shift in DMSO HRS vibrational modes as function of H_2O concentration.

HRS of DMSO (cm^{-1})	75 % DMSO (cm^{-1})	50 % DMSO (cm^{-1})	33.3 % DMSO (cm^{-1})	10 % DMSO (cm^{-1})	Assignment
306	-0.4 ± 1.1	0.9 ± 1.0	-0.5 ± 1.0	-2.2 ± 0.9	C-S-C bending
336	1.3 ± 1.1	5.3 ± 1.1	7.8 ± 1.0	11.7 ± 1.2	C-S=O rocking (out-of-plane)
383	0.5 ± 0.2	3.3 ± 0.2	4.5 ± 0.2	6.4 ± 0.2	C-S=O rocking (in-plane)
667	2.0 ± 0.6	5.3 ± 0.4	7.0 ± 0.4	9.4 ± 0.3	C-S stretching (sym.)
696	2.5 ± 0.3	7.1 ± 0.2	10.1 ± 0.2	14.1 ± 0.2	C-S stretching (asym.)
954	-0.4 ± 0.8	-0.1 ± 0.8	-1.8 ± 0.7	-2.2 ± 0.7	C-H rocking
1290	2.1 ± 0.1	6.9 ± 0.1	8.2 ± 0.1	11.0 ± 0.5	H-C-H bending
1310	2.2 ± 0.1	6.6 ± 0.1	7.5 ± 0.1	10.2 ± 0.1	H-C-H bending
1417	0.6 ± 0.3	0.3 ± 0.3	0.6 ± 0.3	1.0 ± 0.3	H-C-H bending
1442	-0.6 ± 0.1	0.2 ± 0.1	-1.3 ± 0.1	0.0 ± 0.1	H-C-H bending
2915	1.7 ± 0.1	5.6 ± 0.1	8.2 ± 0.1	13.9 ± 0.1	C-H stretching (sym.)
2998	1.4 ± 0.3	4.4 ± 0.3	6.4 ± 0.3	10.7 ± 0.3	C-H stretching (asym.)

Abbreviations: sym=symmetric; asym=asymmetric

3.4 Effect of H_2O on the C-S Bonds of DMSO

In Fig. S7, the amplitude normalized HRS spectra of the symmetric and antisymmetric C-S stretch modes are shown. The peak areas and peak wavenumbers of the symmetric and antisymmetric C-S stretch modes are plotted in Fig. S8.

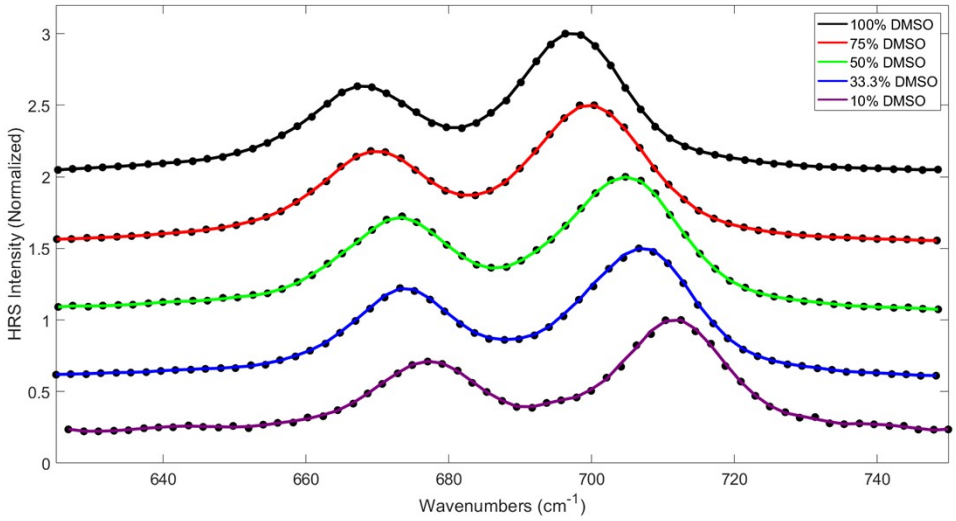

Fig. S7. The hyper-Raman spectra of the symmetric and antisymmetric C-S stretch modes of DMSO in solution. Note the individual data points are shown as black dots and the lines are rendered after passing the data through a Savitzky-Golay filter.

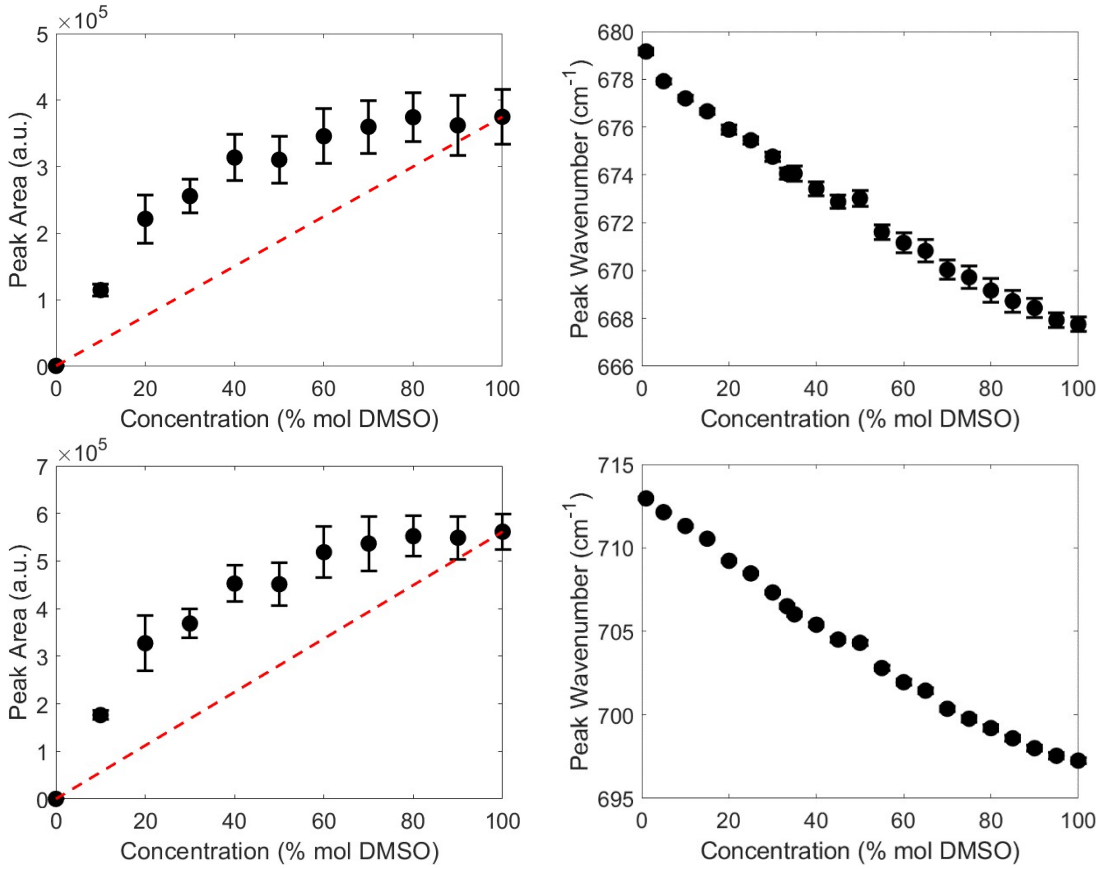

Fig. S8. Plot of the peak area (left) and wavenumber (right) of the C-S stretch modes (symmetric above, asymmetric below).

3.5 Effect of H_2O on the C-H Bonds of DMSO

In Fig. S9, the amplitude normalized HRS spectra of the C-H rocking mode, and C-H stretching modes are shown. The peak areas and peak wavenumbers of the C-H rocking mode, and C-H stretching modes are plotted in Fig. S10.

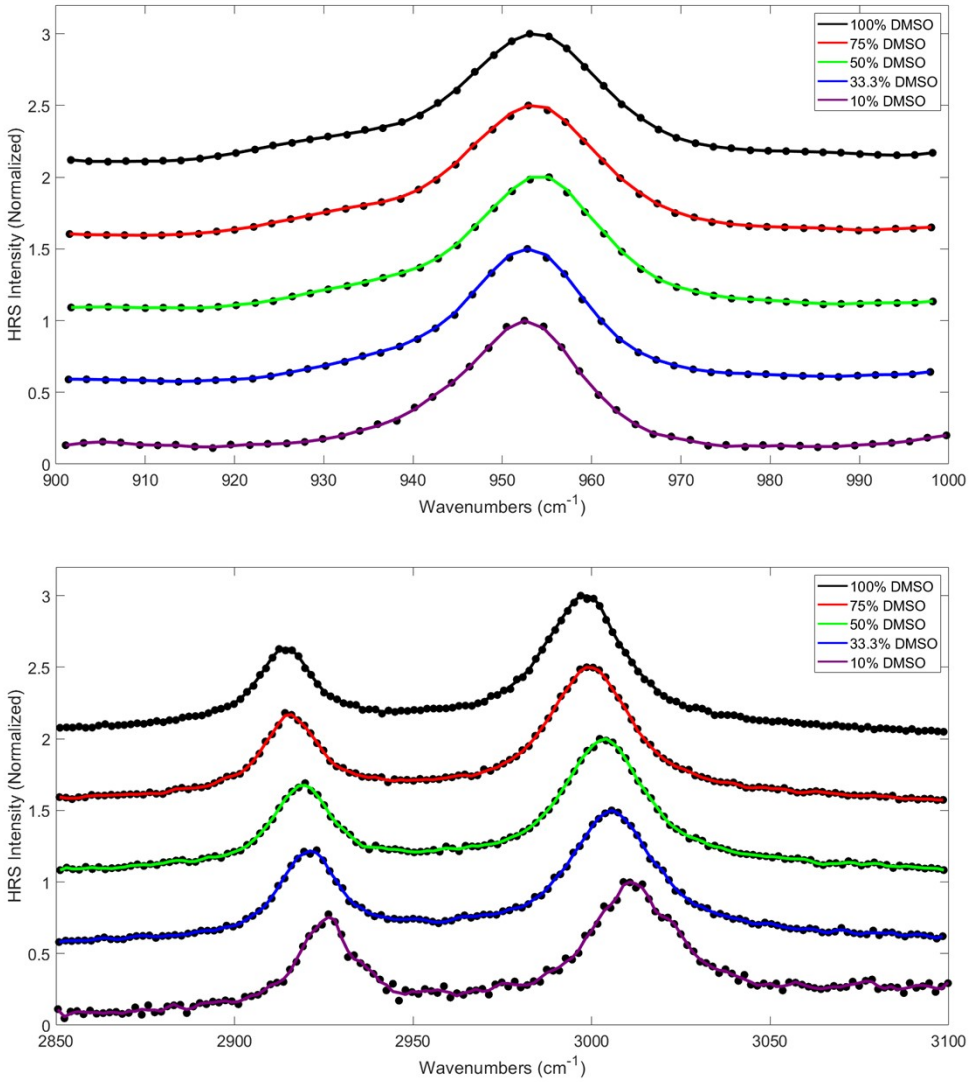

Fig. S9. The hyper-Raman spectra of the C-H rocking mode (top) and C-H stretching modes (bottom) of DMSO in solution. Note the individual data points are shown as black dots and the lines are rendered after passing the data through a Savitzky-Golay filter.

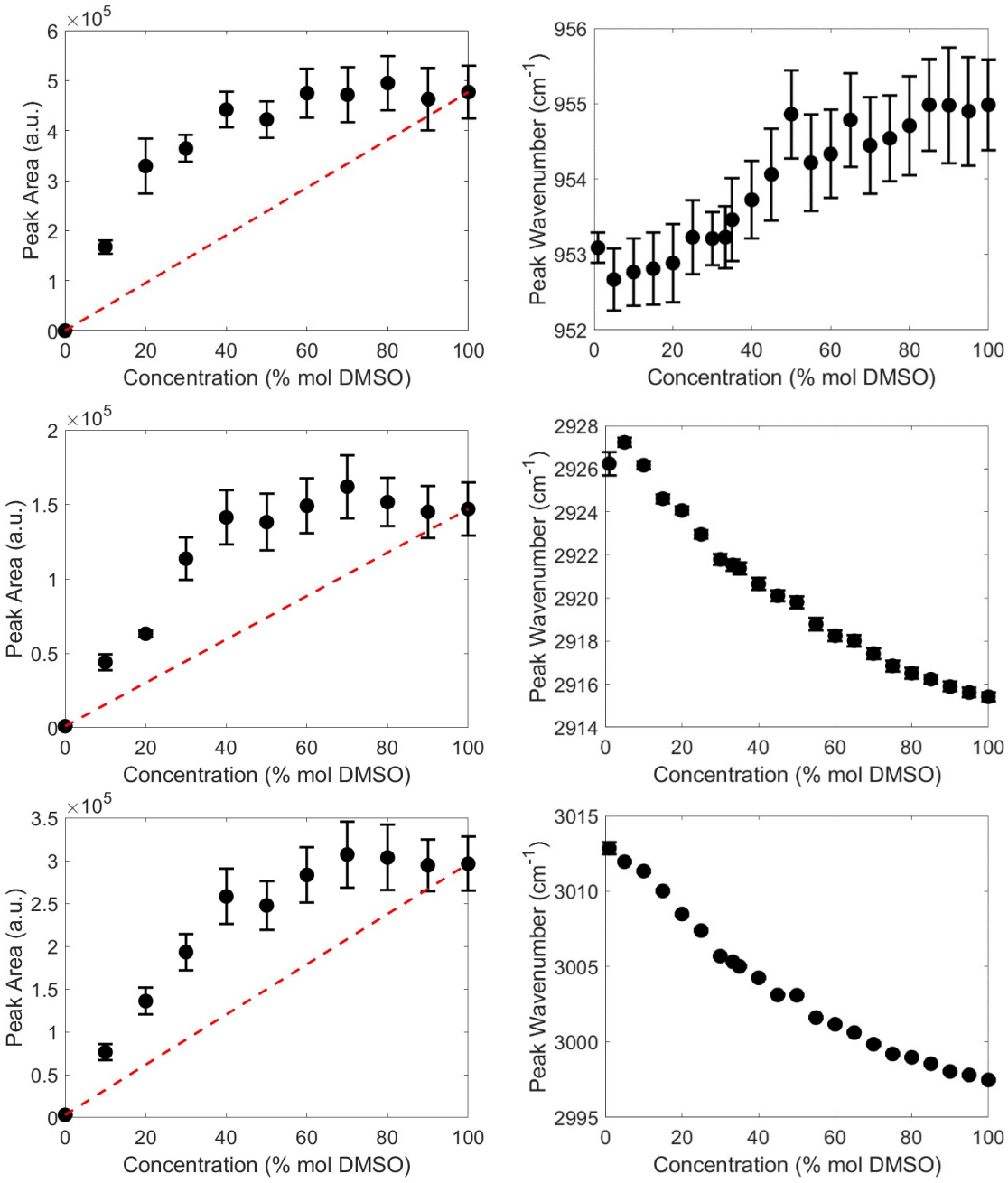

Fig. S10. Plot of the peak area (left) and wavenumber (right) of the C-H rocking mode at 954 cm^{-1}, and C-H stretching modes at 2915 cm^{-1} and 2998 cm^{-1}.

3.6 Effect of DMSO on H_2O Libration, Bend and Stretch Modes

In Fig. S11, the amplitude normalized HRS spectra of the H_2O libration, bend and stretch modes are shown. The peak areas of the H_2O libration, bend and stretch modes are plotted in Fig. S12. Note at high DMSO concentrations the peak fitting algorithm struggles to identify and quantify the ~500 cm^{-1} libration, ~750 cm^{-1} libration, 1655 cm^{-1} bend and ~3330 cm^{-1} stretch mode from the DMSO background.

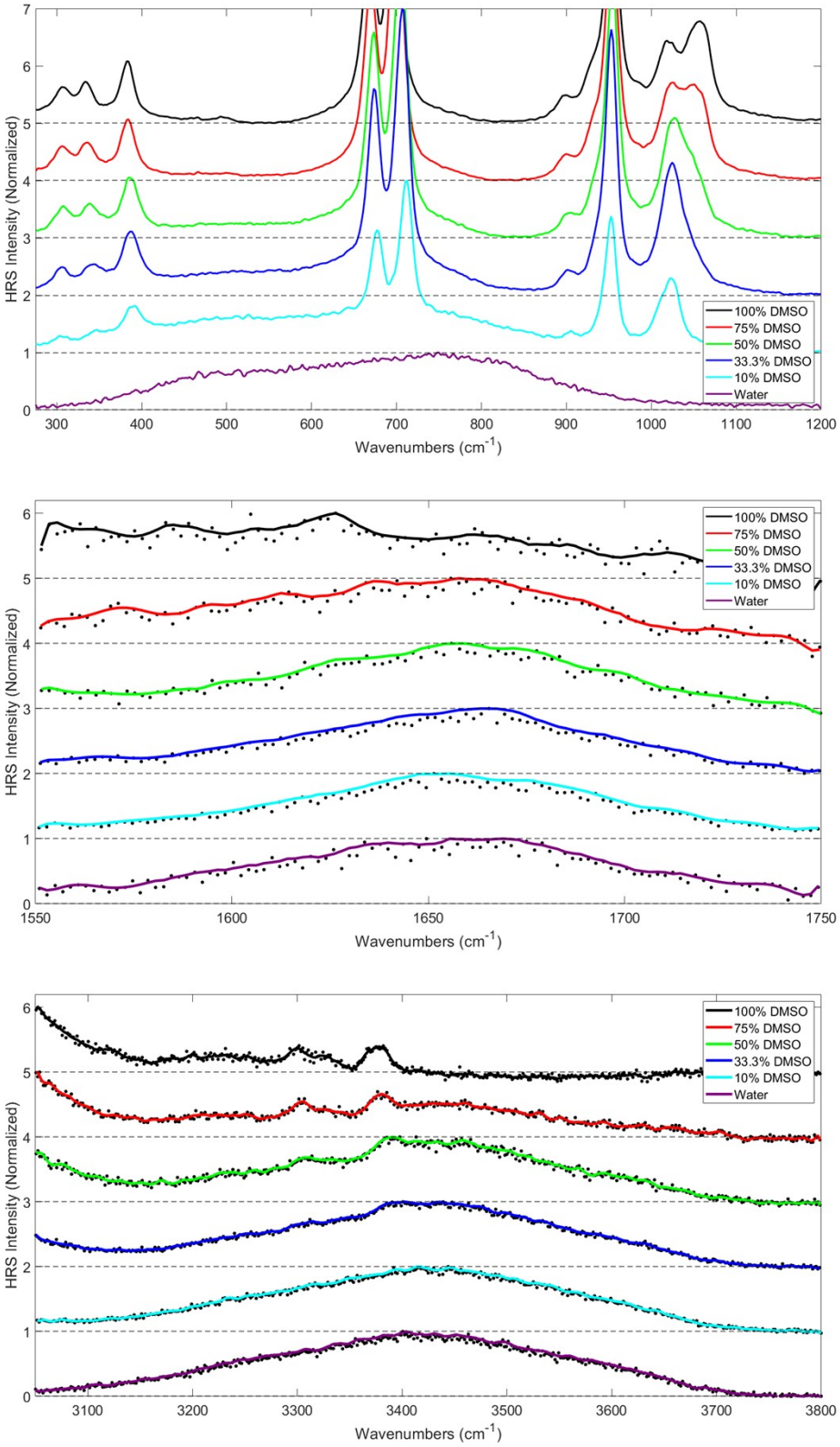

Fig. S11. The hyper-Raman spectra of the H_2O librational modes (top), H_2O bend mode (middle), and the H_2O stretch modes (bottom). Note the individual data points are shown as black dots and the lines are rendered after passing the data through a Savitzky-Golay filter.

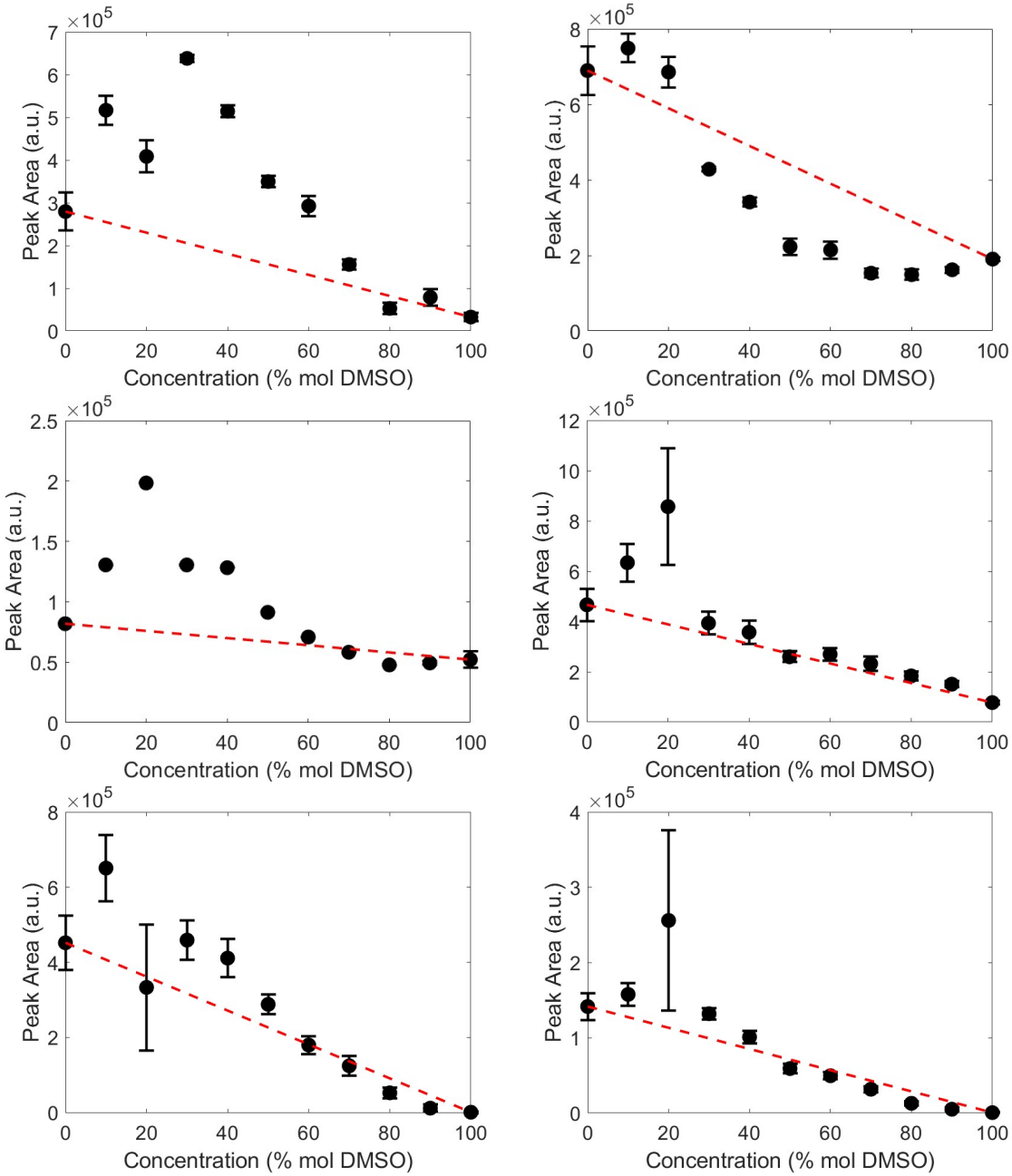

Fig. S12. The peak areas for the H_2O librational modes at ~500 cm^{-1} (top left) and ~750 cm^{-1} (top right), H_2O bend mode at 1655 cm^{-1} (middle left), and the H_2O stretch modes at ~3330 cm^{-1} (middle right), ~3460 cm^{-1} (bottom left), and ~3600 cm^{-1} (bottom right).

References

1 C. B. Marble, X. Xu, K. S. Marble, G. I. Petrov, D. Wang and V. V. Yakovlev, *In Proc. SPIE 11252*, Proc. SPIE, 2020, 28.

2 R. Arora, G. I. Petrov, J. Liu and V. V. Yakovlev, *J. Biomed. Opt.*, 2011, **16**, 021114.

3 V. Korepanov, C. C. Yu and H. Hamaguchi, *J. Raman Spectrosc.*, 2018, **49**, 1742–1746.

4 W. N. Martens, R. L. Frost, J. Kristof and J. Theo Kloprogge, *J. Raman Spectrosc.*, 2002, **33**, 84–91.

5 K.-I. Oh, K. Rajesh, J. F. Stanton and C. R. Baiz, *Angew. Chemie*, 2017, **129**, 11533–11537.

6 V. M. Wallace, N. R. Dhumal, F. M. Zehentbauer, H. J. Kim and J. Kiefer, *J. Phys. Chem. B*, 2015, **119**, 14780–14789.

7 A. L. Smith, *The Coblentz Society Desk Book of Infrared Spectra*, The Coblentz Society, Kirkwood, 2nd edn., 1982.

8 X. Xu, C. B. Marble, G. I. Petrov, D. Wang and V. V. Yakovlev, *In Proc. SPIE 11252*, Proc. SPIE, 2020, 63.